Radial source flows in porous media: Linear stability analysis of axial and helical perturbations in miscible displacements

Amir Riaz and Eckart Meiburg[a)]
Department of Mechanical and Environmental Engineering, University of California, Santa Barbara, California 93106

(Received 20 September 2002; accepted 8 January 2003; published 4 March 2003)

Linear stability results are presented for axial and helical perturbation waves in radial porous media displacements involving miscible fluids of constant density. A numerical eigenvalue problem is formulated and solved in order to evaluate the relevant dispersion relations as functions of the Peclet number and the viscosity ratio. In contrast to the constant algebraic growth rates of purely azimuthal perturbations [C. T. Tan and G. M. Homsy, Phys. Fluids **30**, 1239 (1987)], axial perturbations are seen to grow with a time-dependent growth rate. As a result, there exists a critical time up to which the most dangerous axial wavenumbers are larger, and beyond which the most dangerous azimuthal wavenumbers have higher values. This raises the possibility that early on, the smaller flow scales appear in the axial direction, whereas the later flow stages are dominated by smaller azimuthal features. By rescaling the axial wavenumber, the explicit appearance of time can be eliminated. The maximum growth rate of axial perturbations, as well as their most dangerous and cutoff wavenumbers, are seen to increase with the Peclet number and the viscosity ratio. The most dangerous wavenumber is observed to shift towards the lower end of the spectrum as the Peclet number increases. With increasing viscosity contrast, it first moves towards the lower part of the spectrum, only to shift towards the higher end later on. In the limit of large Pe, asymptotic solutions are obtained for the growth of axial disturbances. Numerical solutions of the full eigenvalue problem generally show good agreement with these asymptotic solutions for large Peclet numbers. Over the entire range of wave vector directions between the purely axial and azimuthal extrema, helical waves display an approximately constant maximum growth rate. The wavenumber of maximum growth as well the maximum growth rate of helical waves can be evaluated from the corresponding purely azimuthal and axial problems. This suggests that in three-dimensional flows the nature of the initial conditions plays an important role.
[DOI: 10.1063/1.1556292]

I. INTRODUCTION

Unstable displacements in porous media have been the subject of intense research for many years, due to their importance in practical applications, for example, in the areas of enhanced oil recovery and ground water hydrology.[1] In an unfavorable mobility gradient, the interface between the two fluids becomes unstable, with the spectrum of unstable wavelengths determined by diffusion or surface tension, depending on whether the displacement is miscible or immiscible, respectively. Pioneering work on the fundamental instability of the displacement process was performed by Hill,[2] Saffman and Taylor,[3] and Chouke, van Meurs, and van der Poel.[4]

In the presence of diffusion or dispersion, the linear stability analysis of miscible flows has to deal with the existence of a time-dependent base state. Towards this end, Tan and Homsy[5,6] developed a quasi-steady-state approximation (QSSA) in order to analyze the stability of miscible displacements in rectilinear domains. The QSSA requires that the temporal change in the base state is slow compared to that of the perturbations. It has been successfully employed in studying the stability characteristics of a variety of miscible flow problems in rectilinear porous media domains, e.g., displacements with nonmonotonic viscosity profiles,[7] vertical miscible displacements with density, stratification,[8] and displacements with shear across the interface.[9]

Miscible displacements caused by radially outward flows from localized sources are of particular importance in oil recovery applications. Linear stability analyses of azimuthal disturbances in radial source flows confined to plane geometries have been carried out for both miscible and immiscible situations.[6,10,11] The growth rate in these cases is known to be algebraic, in contrast to the exponential growth observed for rectilinear flows. Radial displacements furthermore are subject to a critical Peclet number, and they give rise to disturbances that grow in a self-similar fashion.[6]

To our knowledge, the stability of axial and helical perturbations in radial source flows has not yet been analyzed. However, in any three-dimensionally evolving radial source flow, such disturbances can be expected to play an important role,[12] especially in the presence of density variations,[13,14] so

a)Author to whom correspondence should be addressed. Electronic mail: meiburg@engineering.ucsb.edu

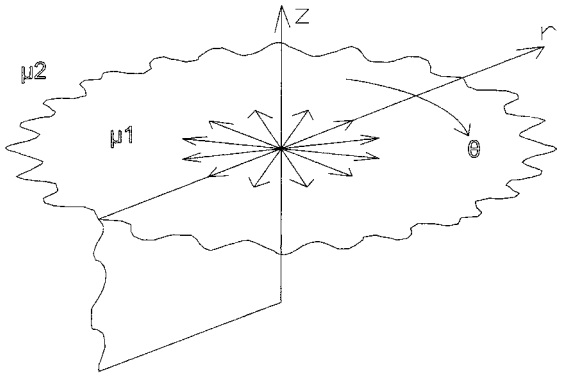

FIG. 1. Principal sketch of the flow domain. Perturbations are considered in the axial z- and the azimuthal θ directions.

that it is essential to obtain information about their linear growth, as well as any nonlinear interactions among them. To this end, we carry out a linear stability analysis of axial and helical disturbances in axisymmetric, radial base flows. After stating the basic assumptions and setting up the corresponding system of governing equations, the linear stability problem will be formulated. Results will be discussed for axial and helical waves in terms of dispersion relations. These provide both the maximum growth rates, as well as the most dangerous and the cutoff wavenumbers. Of particular interest is a comparison between the rescaled, purely axial perturbations on one hand, and the purely azimuthal perturbations considered by Tan and Homsy.[6]

II. MATHEMATICAL FORMULATION

A. Governing equations

We consider a three-dimensional domain, Fig. 1, with a radial line source of strength Q per unit depth. The permeability field is assumed to be constant and diffusion isotropic, while the fluids are considered to be neutrally buoyant and incompressible. As a result, the governing equations take the form

$$\nabla \cdot \mathbf{u} = 0, \tag{1}$$

$$\nabla p = -\frac{\mu}{k}\mathbf{u}, \tag{2}$$

$$\frac{\partial c}{\partial t} + \mathbf{u}\cdot\nabla c = D\nabla^2 c. \tag{3}$$

Here, c denotes the concentration, $\mathbf{u}$ represents the Darcy velocity, and k indicates the permeability. $\mu(c)$ gives the viscosity as a function of the local concentration, and the diffusion coefficient D is taken constant. In assuming a constant value of D, we neglect the effects of velocity-induced dispersion, cf. Taylor.[15] These are known to be relevant in porous media, and both Yortsos and Zeybek,[16] as well as Zimmerman and Homsy,[17] have attempted to account for them on the basis of a Taylor dispersion tensor. However, this approach is strictly applicable only to constant viscosity and density displacements. Petitjeans *et al.*[18] show that it does not correctly predict the velocity-induced dispersion encountered in variable viscosity displacements in a Hele-Shaw cell, for example. As a result, rather than applying a model that may not capture the true physics, we decide to follow the original approach by Tan and Homsy[6] and disregard velocity-induced dispersion for now. This also has the advantage that it allows us to compare the current results for axial waves with their original results for azimuthal waves. However, we would like to mention that we are currently working towards developing improved dispersion models for variable density and viscosity displacements in narrow gaps (Graf *et al.*[19]) and capillary tubes (Wilhelm and Meiburg[20]).

In rendering the above equations dimensionless, we take a slightly different perspective from the one employed by Tan and Homsy.[6] Due to the absence of an external characteristic length, those authors refer all lengths to $d=\sqrt{k}$, i.e., to a length scale related to the microscopic structure of the porous medium. In this way, they arrive at the time scale k/Q, the characteristic velocity $Q/\sqrt{k}$, and the characteristic pressure $Q\mu_1/k$. One might argue that this length scale describing the microstructure of the porous medium is not appropriate for rendering the continuum velocity and time dimensionless. For example, a characteristic velocity U^* in the axisymmetric flow field generated by a point source would be Q/L, with L being the distance from the point source, rather than $Q/\sqrt{k}$. Consequently, we introduce an unspecified global length scale L, in order to obtain the time scale L^2/Q, and the velocity scale Q/L, cf. also the nonlinear simulations by Chen and Meiburg[21] in the quarter five-spot geometry, which does exhibit a global length scale. The characteristic pressure scales with $Q\mu_1/k$, and all viscosities are referred to μ_1. The equations in nondimensional form thus are

$$\frac{1}{r}\frac{\partial}{\partial r}(ru) + \frac{1}{r}\frac{\partial v}{\partial \theta} + \frac{\partial w}{\partial z} = 0, \tag{4}$$

$$\frac{\partial p}{\partial r} = -\mu u, \tag{5}$$

$$\frac{\partial p}{\partial \theta} = -r\mu v, \tag{6}$$

$$\frac{\partial p}{\partial z} = -\mu w, \tag{7}$$

$$\frac{\partial c}{\partial t} + u\frac{\partial c}{\partial r} + \frac{v}{r}\frac{\partial c}{\partial \theta} + w\frac{\partial c}{\partial z} = \frac{1}{\mathrm{Pe}}\left(\frac{\partial^2 c}{\partial r^2} + \frac{1}{r}\frac{\partial c}{\partial r} + \frac{1}{r^2}\frac{\partial^2 c}{\partial \theta^2} + \frac{\partial^2 c}{\partial z^2}\right). \tag{8}$$

It should be pointed out that, in spite of introducing an artificial global length scale L, we arrive at the same set of dimensionless equations as Tan and Homsy,[6] since all factors of L cancel out in the process of nondimensionalization. The Peclet number $\mathrm{Pe}=Q/D$ appears as the only dimensionless parameter in the above equations so far. Another parameter will arise later due to the concentration dependence of viscosity. An axisymmetric solution to the above equations is given by[6]

$$u_o = \frac{1}{r}, \tag{9}$$

$$v_o = w_o = 0, \tag{10}$$

$$c_o = \frac{\int_0^{r\sqrt{\mathrm{Pe}/2t}} s^{(\mathrm{Pe}-1)} e^{-s^2/2} ds}{\int_0^{\infty} s^{(\mathrm{Pe}-1)} e^{-s^2/2} ds}. \tag{11}$$

An order $\mathcal{O}(1/\sqrt{\mathrm{Pe}})$ approximation to the above base concentration valid for large value of Pe is[6]

$$c_o = \frac{1}{2}\left\{1 + \mathrm{erf}\left(r\sqrt{\frac{\mathrm{Pe}}{2t}} - \sqrt{\mathrm{Pe}}\right)\right\}. \tag{12}$$

Below, we will employ Eq. (11) for stability analyses in the range $\mathrm{Pe} \leqslant 100$, and Eq. (12) for higher values of Pe. In this context, it is appropriate to discuss representative values of Pe in practical applications. One can write

$$\mathrm{Pe} = \frac{Q}{D} = \frac{U^* L}{D} = \frac{U^* d}{D}\frac{L}{d} = \mathrm{Pe}_d \frac{L}{d}, \tag{13}$$

where Pe_d is the Peclet number formed with the pore scale d, and L/d is the ratio of macroscopic to microscopic length scales. It is well known that Pe_d is an $O(1)$ quantity in both the diffusion and the dispersion dominated regimes, cf. Taylor.[15] However, L/d can be very large, with the macroscopic length scale L (such as the distance of the front from the injection well) on the order of meters or more, and the pore scale on the order of millimeters or less. Hence, the Peclet number as defined in the present investigation, i.e., $\mathrm{Pe} = Q/D$, can easily reach values of $O(10^3)$ or more.

B. Linear stability problem

In order to carry out the linear stability analysis, the dependent variables are decomposed into base and disturbance components as $x = x_o + x'$. By making this substitution in the above equations, subtracting out the base state, and neglecting higher order terms, we obtain the following linearized equations for the disturbances:

$$\frac{1}{r}\frac{\partial}{\partial r}(ru') + \frac{1}{r}\frac{\partial v'}{\partial \theta} + \frac{\partial w'}{\partial z} = 0, \tag{14}$$

$$\frac{\partial p'}{\partial r} = -\mu_o u' - \frac{\mu'}{r}, \tag{15}$$

$$\frac{\partial p'}{\partial \theta} = -r\mu_o v', \tag{16}$$

$$\frac{\partial p'}{\partial z} = -\mu_o w', \tag{17}$$

$$\frac{\partial c'}{\partial t} + u'\frac{\partial c_o}{\partial r} + \frac{1}{r}\frac{\partial c'}{\partial r} = \frac{1}{\mathrm{Pe}}\left(\frac{\partial^2 c'}{\partial r^2} + \frac{1}{r}\frac{\partial c'}{\partial r} + \frac{1}{r^2}\frac{\partial^2 c'}{\partial \theta^2} + \frac{\partial^2 c'}{\partial z^2}\right), \tag{18}$$

$$\mu' = \frac{d\mu}{dc}c'. \tag{19}$$

Upon eliminating pressure from Eqs. (15), (16), and (17), and employing Eq. (14) to eliminate w, the equations for u and v can be written as (after omitting the primes)

$$\frac{\partial^2 u}{\partial r^2} + \left(Rc_o' + \frac{1}{r}\right)\frac{\partial u}{\partial r} + \left(Rc_o' - \frac{1}{r}\right)\left(\frac{u}{r} + \frac{1}{r}\frac{\partial v}{\partial \theta}\right) + \frac{1}{r}\frac{\partial^2 v}{\partial r \partial \theta} + \frac{\partial^2 u}{\partial z^2} + \frac{R}{r}\frac{\partial^2 c}{\partial z^2} = 0, \tag{20}$$

$$\frac{\partial v}{\partial r} + \left(Rc_o' + \frac{1}{r}\right)v - \frac{1}{r}\frac{\partial u}{\partial \theta} - \frac{R}{r^2}\frac{\partial c}{\partial \theta} = 0, \tag{21}$$

where $c_o' = dc_o/dr$. R is the second nondimensional parameter in the problem; it represents the viscosity concentration relationship given by

$$R = \ln\left(\frac{\mu_2}{\mu_1}\right) = \frac{1}{\mu}\frac{d\mu}{dc}. \tag{22}$$

Hence

$$\mu(c) = e^{Rc}. \tag{23}$$

The disturbances are decomposed into Fourier modes as

$$(u, v, c)(r, \theta, t) = \left(\frac{\hat{u}}{r}, \frac{\hat{v}}{r}, \hat{c}\right)(r, t) e^{i(m\theta + n(t)z)}. \tag{24}$$

The reason for assuming a time-dependent wavenumber in Eq. (24) will become clear below. We introduce a coordinate transformation involving the similarity variable η and time

$$\eta = r\sqrt{\frac{\mathrm{Pe}}{2t}}, \quad t = t. \tag{25}$$

In analogy to the treatment of azimuthal waves,[6] we search for a separable solution of the form

$$(\hat{u}, \hat{v}, \hat{c})(\eta, t) = (g, h, f)(\eta) s(t). \tag{26}$$

By using Eqs. (24), (25), and (26), the concentration and velocity equations (18), (20), and (21) can be written as

$$\frac{d^2 g}{d\eta^2} + \left(Rc_o' - \frac{1}{\eta}\right)\frac{dg}{d\eta} - \frac{2tn^2}{\mathrm{Pe}}g + im\left(\frac{Rc_o'}{\eta} - \frac{2}{\eta^2}\right)h + \frac{im}{\eta}\frac{dh}{d\eta} - \frac{2tn^2 R}{\mathrm{Pe}}f = 0, \tag{27}$$

$$\frac{dh}{d\eta} + Rc_o' h - \frac{im}{\eta}g - \frac{imR}{\eta}f = 0, \tag{28}$$

$$\frac{d^2 f}{d\eta^2} + \left((1 - \mathrm{Pe})\frac{1}{\eta} + \eta\right)\frac{df}{d\eta} - \frac{1}{\eta^2}m^2 f - \frac{2t}{\mathrm{Pe}}n^2 f + iz2t\frac{dn}{dt}f - \frac{\mathrm{Pe}c_o'}{\eta}g = 2t\frac{1}{s}\frac{ds}{dt}f. \tag{29}$$

The explicit appearance of time in the above equations implies that the variable η is not an exact similarity variable for axial waves, in contrast to the situation for azimuthal waves. Progress can be made with the above equations by assuming a functional form for the axial wavenumber as (Homsy, private communication)

$$n(t)=\frac{1}{\sqrt{2t}}n'. \tag{30}$$

With this definition, the term containing the time derivative of $n(t)$ in Eq. (29) becomes $izfn'/\sqrt{2t}$. We note that this is the only term in which time appears after the substitution of $n(t)$ into Eqs. (27)–(29). Formally the term with dn/dt, being proportional to $1/\sqrt{2t}$, becomes small only for large times. However, comparisons with direct numerical simulations indicate that this term can be neglected even for times of $\mathcal{O}(1)$. The governing equations can then be expressed as

$$\frac{d^2g}{d\eta^2}+\left(Rc_o'-\frac{1}{\eta}\right)\frac{dg}{d\eta}-\frac{n'^2}{\mathrm{Pe}}g+im\left(\frac{Rc_o'}{\eta}-\frac{2}{\eta^2}\right)h + \frac{im}{\eta}\frac{dh}{d\eta}-\frac{n'^2R}{\mathrm{Pe}}f=0, \tag{31}$$

$$\frac{dh}{d\eta}+Rc_o'h-\frac{im}{\eta}g-\frac{imR}{\eta}f=0, \tag{32}$$

$$\frac{d^2f}{d\eta^2}+\left((1-\mathrm{Pe})\frac{1}{\eta}+\eta\right)\frac{df}{d\eta}-\frac{1}{\eta^2}m^2f-\frac{n'^2}{\mathrm{Pe}}f-\frac{\mathrm{Pe}c_o'}{\eta}g=\sigma f, \tag{33}$$

with the boundary conditions

$$(f,g,h)(\eta\to\pm\infty)=0. \tag{34}$$

Equations (31)–(34) form a linear eigenvalue system with an eigenvalue σ given by

$$\sigma(m,n,\mathrm{Pe},R)=2t\frac{1}{s}\frac{ds}{dt}. \tag{35}$$

As for azimuthal waves,[6] we find that helical disturbances grow algebraically $\propto t^{\sigma/2}$. The original axial wavenumber $n(t)$ for different times can be obtained from relation (30). In this context, it is important to appreciate a fundamental difference between azimuthal and axial perturbation waves, respectively. The azimuthal wavelength naturally increases with $t^{1/2}$ as the front moves radially outward from the source. A corresponding stretching mechanism for increasing the wavelength of axial perturbations is absent, which results in the need to scale the axial wavenumber with $t^{1/2}$.

The above eigenvalue problem is solved numerically by means of the public domain subroutine packages LAPACK and ARPACK,[22,23] with 10th-order discretization of the derivatives using compact finite differences.[24] The real part of the complex growth constant σ represents the algebraic growth rate of the disturbances.

The plane, two-dimensional case for purely azimuthal disturbances considered by Tan and Homsy[6] is recovered by setting $n'=0$. In the above notation, the resulting equations read

$$\frac{d^2g}{d\eta^2}+\left(Rc_o'+\frac{1}{\eta}\right)\frac{dg}{d\eta}-\frac{m^2}{\eta^2}g=R\frac{m^2}{\eta^2}f, \tag{36}$$

$$\frac{d^2f}{d\eta^2}+\left[(1-\mathrm{Pe})\frac{1}{\eta}+\eta\right]\frac{df}{d\eta}-\left(\frac{m^2}{\eta^2}+\sigma\right)f=\frac{\mathrm{Pe}}{\eta}c_o'g. \tag{37}$$

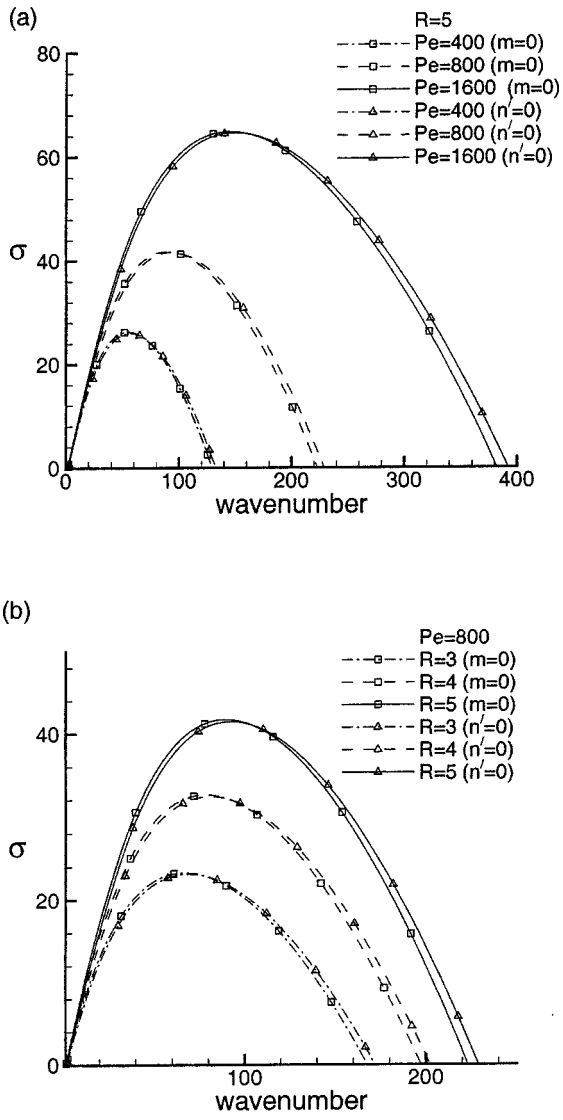

FIG. 2. Dispersion relations for purely azimuthal ($n'=0$) and purely axial ($m=0$) perturbation waves, respectively, as functions of (a) Pe and (b) R. Rescaling the axial wavenumber with $n'=n\sqrt{2t}$ results in very similar dispersion relations for the two cases. The maximum growth rate, as well as the maximum and cutoff wavenumbers, increase with Pe and R.

Conversely, for the case of purely axial perturbations ($m=0$), we obtain

$$\frac{d^2g}{d\eta^2}+\left(Rc_o'-\frac{1}{\eta}\right)\frac{dg}{d\eta}-\frac{n^2}{\mathrm{Pe}}g=R\frac{n^2}{\mathrm{Pe}}f, \tag{38}$$

$$\frac{d^2f}{d\eta^2}+\left[(1-\mathrm{Pe})\frac{1}{\eta}+\eta\right]\frac{df}{d\eta}-\left(\frac{n^2}{\mathrm{Pe}}+\sigma\right)f=\frac{\mathrm{Pe}}{\eta}c_o'g. \tag{39}$$

These two sets of equations have closely related structures. As we will see below, this is responsible for the fact that the dispersion relationships of purely axial and purely azimuthal perturbations are quantitatively quite similar.

III. RESULTS

The two dimensionless parameters governing the linear stability problem are the Peclet number Pe and the mobility ratio R. Figure 2 demonstrates their influence on the disper-

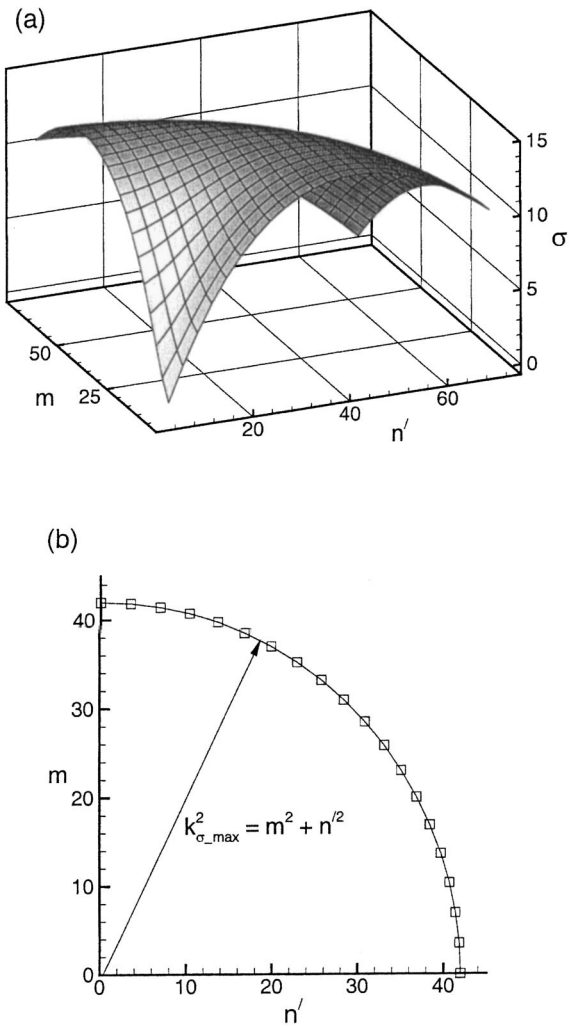

FIG. 3. Dispersion relations for helical perturbations at Pe=400, $R=3$. (a) The growth rate σ is plotted as a surface above the m, n' plane. (b) Trajectory of the maximum growth rate in the m, n' plane. Along the $n'=0$ and $m=0$ axes, the maximum growth rate corresponds to the two-dimensional plane and axisymmetric cases, respectively. For helical perturbations with $(m,n'\neq 0)$, the wavenumber $k_{\sigma_{\max}}$ of maximum growth follows an elliptical path in the m, n' plane.

sion relations for purely axial and azimuthal perturbations, respectively. The growth rates for azimuthal perturbations, obtained when $n'=0$, closely reproduce those of Tan and Homsy,[6] which validates the present computational procedures for solving the eigenvalue problem.

When comparing purely axial with azimuthal perturbations, we note that the shapes of the respective dispersion relationships in general, and the maximum growth rates in particular, are quite similar for the entire range of Pe and R. The maximum growth rate increases with increasing values of Pe and R, while the most dangerous and cutoff wavenumbers shift to higher values.

Figure 3(a) shows that the maximum growth rates of helical modes $(m,n'\neq 0)$ are very close to those of the purely azimuthal and axial modes. The trajectory of maximum growth for helical perturbations in the m, n' plane is plotted in Fig. 3(b). It is seen to closely follow an elliptical path given by

$$\frac{m^2}{m^2_{\sigma_{\max}}|_{n'=0}}+\frac{n'^2}{n'^2_{\sigma_{\max}}|_{m=0}}=1. \tag{40}$$

The above graph suggests that for helical modes with wavenumber $k=\sqrt{m^2+n'^2}$, the maximum growth rates and the corresponding wavenumbers can be estimated with good accuracy from the purely axial and azimuthal problems with corresponding wavenumbers. It furthermore demonstrates that there are no preferred helical modes, so that in a fully three-dimensional flow the entire range of helical modes between the purely axial and azimuthal extrema can be amplified. Under these circumstances, the characteristics of the initial conditions can take on special importance.

A. Relationship between purely axial and azimuthal modes

The dispersion relations plotted in Fig. 2 suggest that the characteristics of the azimuthal and axial modes are closely related, at least in the limit of large Pe. In order to further investigate this issue, we derive an analytic solution for axial waves in the limit of large Pe, similar to the one presented by Tan and Homsy[6] for azimuthal perturbations. To this end, we set $m=0$ in Eqs. (31)–(33) and introduce a modified wavenumber

$$n_1=n'\mathrm{Pe}^{-1/2},$$

along with a modified growth rate

$$\sigma_1=\frac{\sigma}{\sqrt{\mathrm{Pe}}}.$$

Upon setting

$$\eta=x+\sqrt{\mathrm{Pe}},$$

and eliminating f from Eqs. (31) and (33), we obtain

$$\frac{d^2g}{dx^2}+Rc_o'\frac{dg}{dx}-n_1^2\left(1-\frac{Rc_o'}{\hat{\sigma}}\right)g+\mathcal{O}(\mathrm{Pe}^{-1/2})=0, \tag{41}$$

where

$$\hat{\sigma}=\sigma_1+\frac{n_1^2}{\sqrt{\mathrm{Pe}}}.$$

Equation (41) is identical to the one derived by Tan and Homsy[1] for purely azimuthal disturbances in the limit of large Pe. Of course, the wavenumber is defined differently here. An analytical solution of Eq. (41) is presented by both Hickernell and Yortsos,[25] as well as Tan and Homsy.[6] For the present case of axial perturbations, and in the limit of large n_1 we obtain

$$\sigma_1=\frac{R}{\sqrt{\pi}}\left(1-\frac{1}{n_1}\right)-\frac{n_1^2}{\sqrt{\mathrm{Pe}}}+\mathcal{O}(n_1^{-2}), \tag{42}$$

with the most dangerous wavenumber

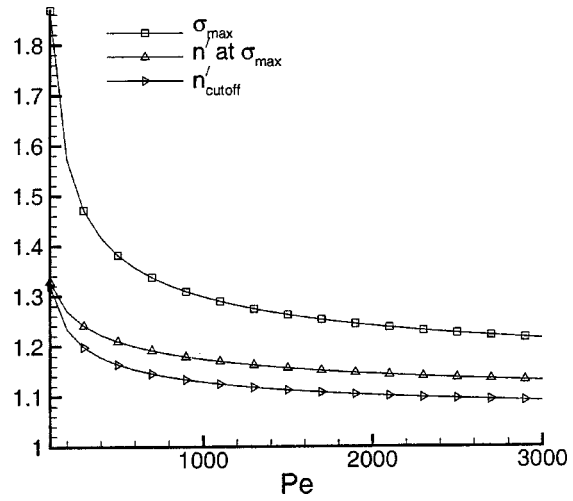

FIG. 4. Ratios of asymptotic to numerical values as a function of Pe ($R=5$) for the maximum growth rate, the most dangerous axial wavenumber and the cutoff axial wavenumber. All ratios approach unity for large Pe.

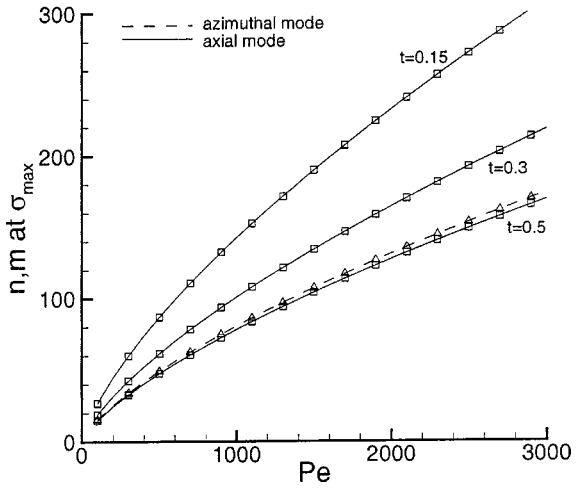

FIG. 5. Original wavenumber n of maximum growth as a function of Pe at $R=3$ for different times. The most dangerous wavenumber of the axial perturbations starts at a magnitude higher than that of the most dangerous azimuthal perturbations. Its magnitude decreases with time and becomes approximately equal to the magnitude of the most amplified azimuthal perturbation at $t=0.5$.

$$n'_{\max}=\left(\frac{R}{2\sqrt{\pi}}\right)^{1/3}\mathrm{Pe}^{2/3}, \tag{43}$$

the cutoff wavenumber

$$n'_{\mathrm{cutoff}}=\left(\frac{R}{\sqrt{\pi}}\right)^{1/2}\mathrm{Pe}^{3/4}, \tag{44}$$

and the growth rate

$$\sigma_{\max}=\frac{R}{\sqrt{\pi}}\mathrm{Pe}^{1/2}\left\{1-\left(\frac{9\sqrt{\pi}}{4R}\right)^{1/3}\mathrm{Pe}^{-1/6}\right\}. \tag{45}$$

Figure 4 presents the ratios of the above asymptotic values to those obtained numerically for the maximum growth rate $\sigma_{\max}$, the corresponding wavenumber n', and the cutoff wavenumber n'_{cutoff}. As is to be expected, they approach unity as Pe becomes large.

When comparing with the results of Tan and Homsy[6] for azimuthal modes, we find that in the limit of large Pe the ratio of the wavenumbers for purely azimuthal and axial modes is

$$\frac{m_{\max}}{n'_{\max}}=\frac{m_{\mathrm{cutoff}}}{n'_{\mathrm{cutoff}}}=1. \tag{46}$$

We furthermore note that in this limit the ratio of the wavenumbers is independent of the viscosity ratio. The maximum growth rate is identical for axial and azimuthal disturbances.

The original wavenumber n of maximum growth for axial perturbations, which is a function of time as indicated by Eq. (30), shifts to lower values as t is increased. This time dependence is plotted in Fig. 5, based on data calculated numerically from Eqs. (31)–(33). The most dangerous wavenumber for axial perturbations initially has a higher value than that for azimuthal perturbations, but subsequently decreases with time.

Based on numerical solutions of Eqs. (31)–(33), Fig. 6(a) shows the ratio of azimuthal to axial wavenumbers of maximum growth, as well as the ratio of azimuthal to axial cutoff wavenumbers, as functions of Pe. These ratios approach a value of unity as $\mathrm{Pe}\to\infty$. Note that the ratio of the cutoff wavenumbers approaches this limit faster than the ratio of the wavenumbers of maximum growth, due to the different exponents of Pe in Eqs. (43) and (44). Figure 6(b) provides corresponding information as a function of R. Interestingly, a maximum occurs at intermediate R values in the ratio of wavenumbers of maximum growth.

B. Influence of Pe and *R*

Figure 7 compares the results obtained from Eqs. (31)–(33) with the asymptotic relationships for large Pe. The maximum growth rate $\sigma_{\max}$ is seen to increase with Pe and R. For the parameter range shown in the figure, the slope is not yet constant in the log–log plot, as indicated by the slope values at two positions along the curve. However, the computational data clearly approach the proper asymptotic behavior.

The wavenumber corresponding to the maximum growth rate is plotted in Fig. 8 as a function of R and Pe for the axial and azimuthal modes. While the asymptotic dependence on Pe is recovered to a high degree of accuracy, there is a significant discrepancy between the numerical and asymptotic values as a function of R, as can be seen in Fig. 8(b). One possible source of this discrepancy may be the relatively small asymptotic exponent of R in Eq. (43), i.e., 1/3, which raises the possibility that the numerical data are not yet in the asymptotic regime.

Figure 9 depicts the increase of the cutoff wavenumber with Pe and R. Again, good agreement is found with the predicted asymptotic behavior.

The ratio of the cutoff wavenumber to the wavenumber of maximum growth, shown in Fig. 10, displays an interesting behavior. With increasing Pe, the most dangerous wavenumber is seen to shift monotonically towards the lower part

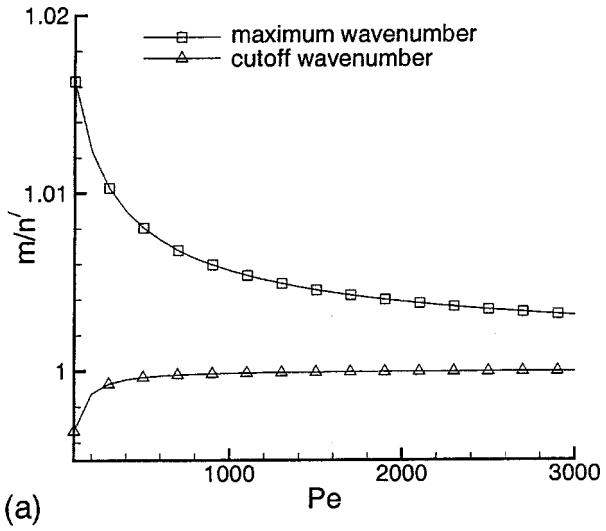

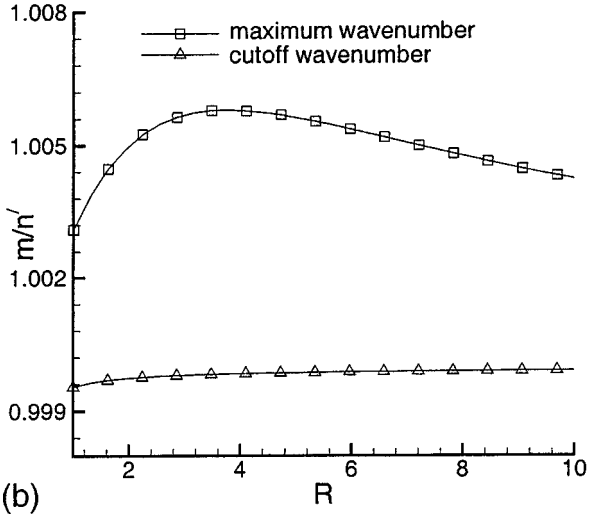

FIG. 6. Ratios of azimuthal to axial, maximum, and cutoff wavenumbers, (a) as function of Pe at $R=5$; (b) as function of R at Pe$=1000$. In (a) both ratios monotonically approach a value of unity as Pe$\rightarrow\infty$. In (b) there is a maximum in the ratio of the most dangerous wavenumbers near $R=4$. At moderate values of Pe and R, the ratio of the most dangerous wavenumbers deviates from the asymptotic limit of unity significantly more then the cutoff wavenumber ratio.

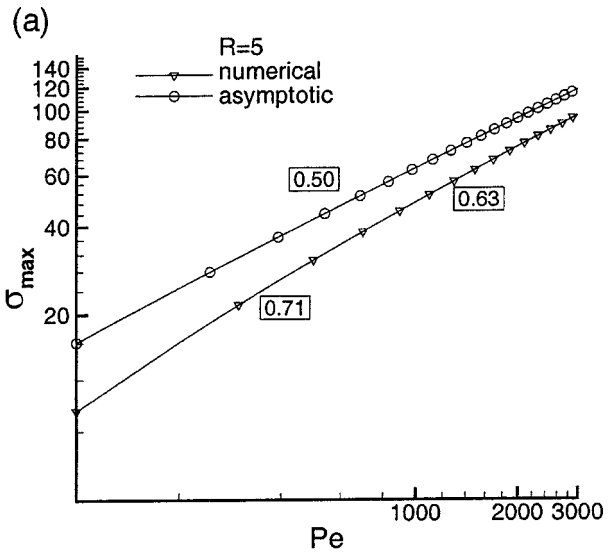

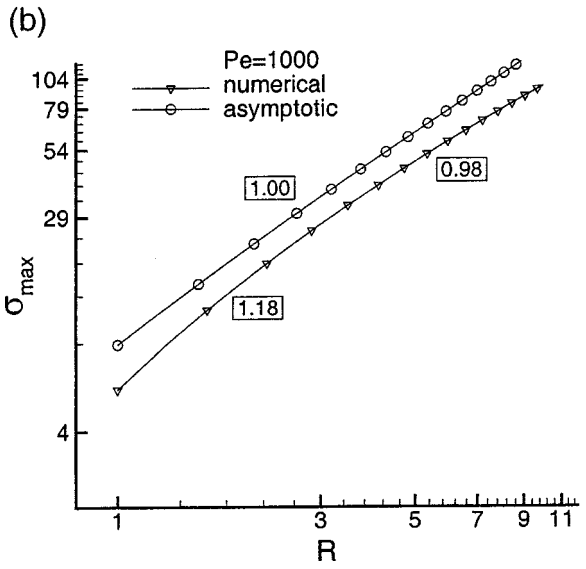

FIG. 7. $\sigma_{\max}$ as a function of (a) Pe for $R=5$; (b) R for Pe$=1000$. The numbers next to the lines specify the respective local slopes. The asymptotic relationship according to Eq. (45) is also plotted. The slopes of the numerical data decrease slightly with increasing Pe and R, and they approach the expected asymptotic behavior.

of the spectrum, cf. Fig. 10(a). In contrast, a maximum of this ratio is observed at intermediate values of R, Fig. 10(b). This indicates that the wavenumber of maximum growth initially moves towards the lower range of the spectrum, but starts to shift towards the higher range around $R=3$.

IV. SUMMARY AND CONCLUSIONS

A linear stability analysis has been performed for axial and helical perturbations in radial porous media displacements involving miscible fluids of constant density. The relevant dispersion relations are evaluated as functions of the Peclet number and the viscosity ratio, by solving a numerical eigenvalue problem. In contrast to purely azimuthal perturbations,[6] whose algebraic growth rate does not depend on time, axial perturbations are seen to grow algebraically with a time-dependent growth rate. However, by rescaling the axial wavenumber appropriately, the explicit appearance of time in the eigenvalue problem can be avoided. The resulting dispersion relationships for axial waves are seen to be qualitatively and quantitatively similar to those for azimuthal waves. The reason for this similarity is shown to lie in the closely related structures of the differential equations governing these cases.

The analysis of helical waves shows that their maximum growth rate is approximately constant over the entire range of wave vector directions between the purely axial and azimuthal extrema, and that both the maximum growth rate and the wavenumber of maximum growth can be obtained from

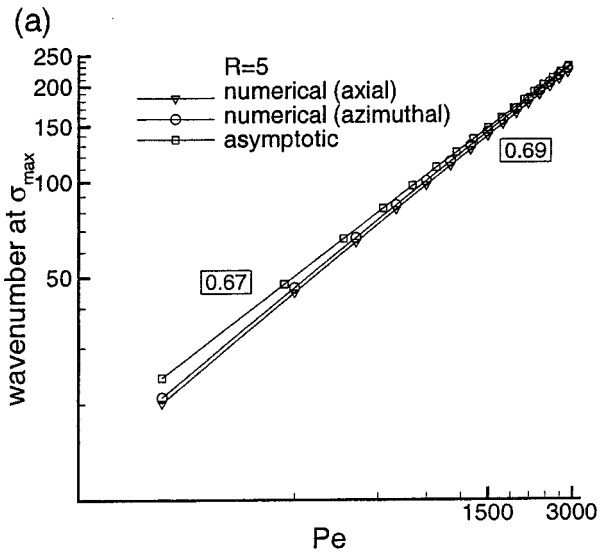

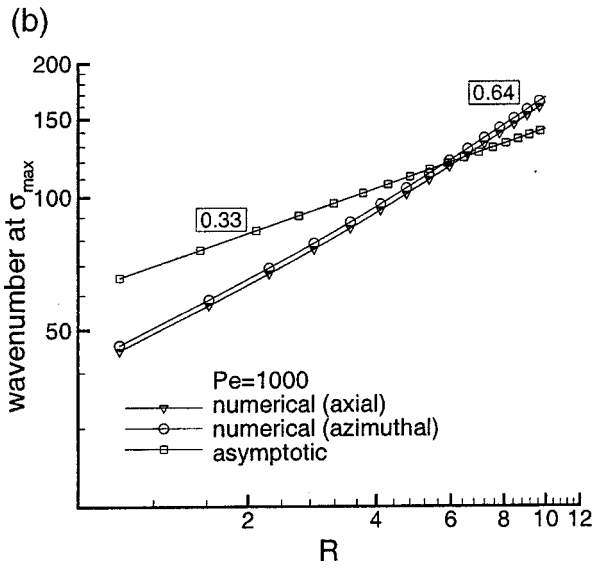

FIG. 8. Wavenumber of maximum growth as a function of (a) Pe and (b) R, for axial and azimuthal perturbations. While the asymptotic dependence on Pe is recovered to a high degree of accuracy, there is a significant discrepancy between the numerical and asymptotic values as a function of R. Possibly, the numerical data are not yet in the asymptotic regime.

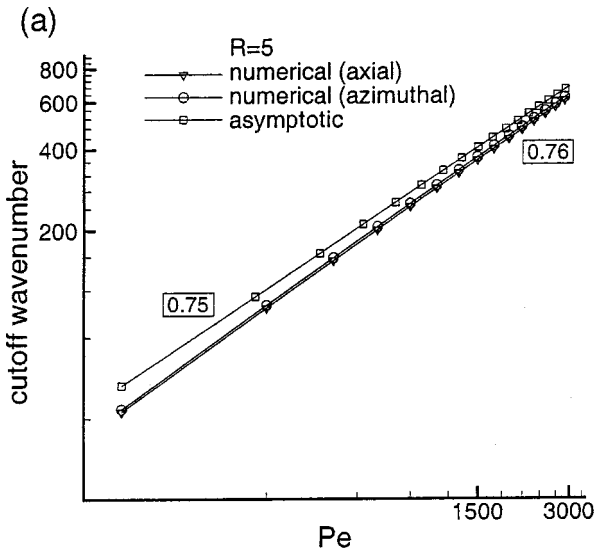

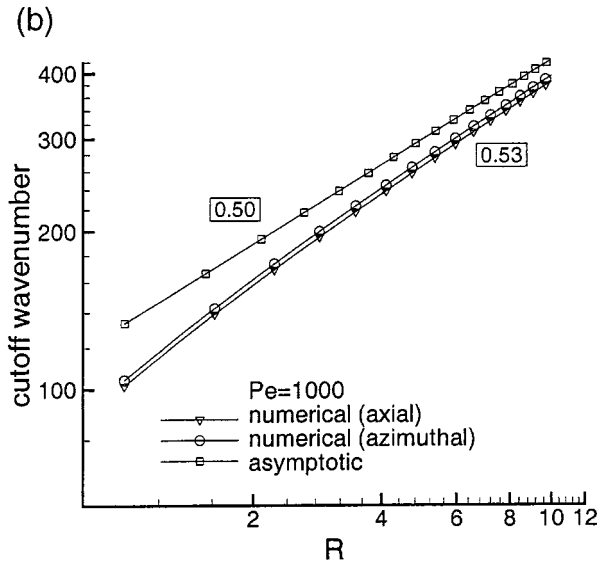

FIG. 9. Cutoff wavenumber as a function of (a) Pe, and (b) R, for axial and azimuthal perturbations. Good agreement with the asymptotic behavior predicted by Eq. (44) is observed in both cases.

the corresponding purely axial and azimuthal problems. This suggests that in a fully three-dimensional flow the characteristics of the initial conditions can take on special importance.

The time-dependent growth rate of axial perturbations represents an interesting phenomenon, as it gives rise to a critical time t_{crit}. For $t<t_{crit}$, the most dangerous axial wavenumbers are larger, whereas for $t>t_{crit}$, the most dangerous azimuthal wavenumbers have higher values. Hence, there exists the possibility that at early times the dominant axial flow structures will be of a smaller scale than the corresponding azimuthal features, and that this trend will reverse itself later on.

The maximum growth rate of axial perturbations, as well as their most dangerous and cutoff wavenumbers, are seen to increase with the Peclet number and the viscosity ratio. The most dangerous wavenumber is observed to shift towards the lower end of the spectrum as the Peclet number increases. With increasing viscosity contrast, it first moves towards the lower end of the spectrum, only to shift towards the higher end later on.

In the limit of large Pe, asymptotic solutions can be obtained for the growth of axial perturbations. Numerical solutions of the full eigenvalue problem generally show good agreement with these asymptotic solutions for large Peclet numbers.

The above features regarding the linear stability of axial and helical waves set the stage for interesting nonlinear dynamics as well. Furthermore, it will be of great interest to study their nonlinear interactions with azimuthal waves. A

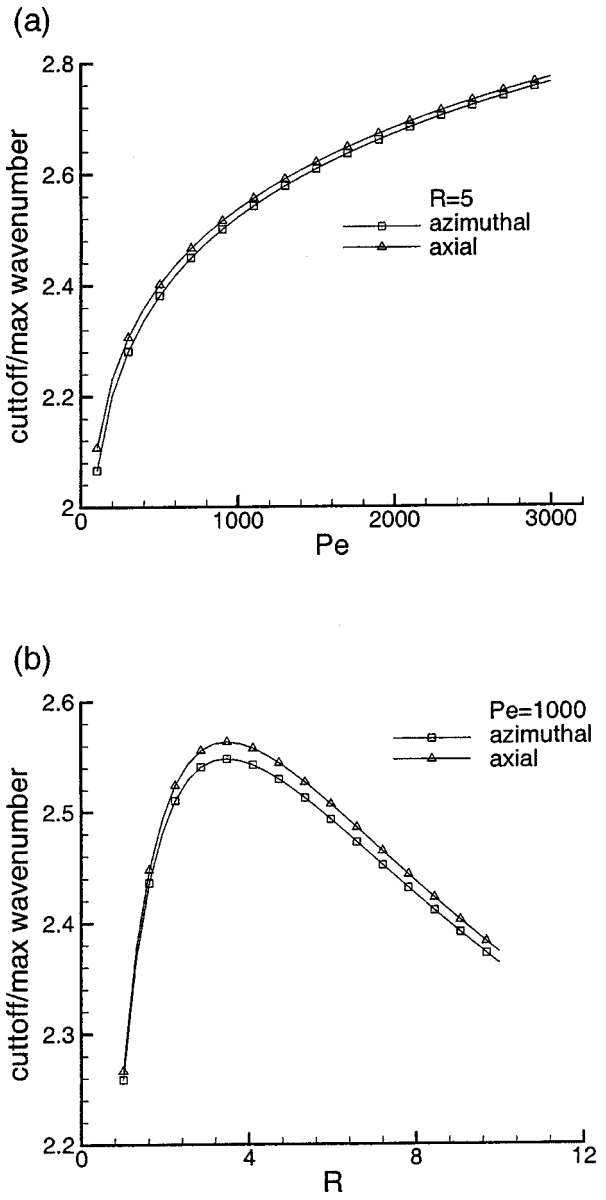

FIG. 10. Ratio of cutoff to most dangerous wavenumber as function of (a) Pe, and (b) *R*, for axial and azimuthal perturbations. The wavenumber of maximum growth shifts monotonically towards the lower part of the spectrum as Pe increases. In contrast, there is a maximum in the ratio of the cutoff to the most dangerous wavenumber as a function of *R*, after which the wavenumber of maximum growth shifts towards the higher end of the unstable spectrum.

numerical study addressing these topics is currently under way.

ACKNOWLEDGMENTS

The authors would like to thank Professor George Homsy for several helpful discussions. Support for this research by the Petroleum Research Fund, the Department of Energy, and an NSF equipment grant is gratefully acknowledged.

[1]G. M. Homsy, ''Viscous fingering in porous media,'' Annu. Rev. Fluid Mech. **19**, 271 (1987).
[2]S. Hill, ''Channeling in packed columns,'' Chem. Eng. Sci. **1**, 247 (1952).
[3]P. G. Saffman and G. I. Taylor, ''The penetration of a fluid into a porous medium or Hele-Shaw cell containing a more viscous liquid,'' Proc. R. Soc. London, Ser. A **245**, 312 (1958).
[4]R. L. Chouke, P. Van Meurs, and C. Van Der Poel, ''The instability of slow, immiscible, viscous liquid–liquid displacements in permeable media,'' Trans. AIME **216**, 188 (1952).
[5]C. T. Tan and G. M. Homsy, ''Stability of miscible displacements in porous media: Rectilinear flows,'' Phys. Fluids **29**, 3549 (1986).
[6]C. T. Tan and G. M. Homsy, ''Stability of miscible displacements in porous media: Radial source flow,'' Phys. Fluids **30**, 1239 (1987).
[7]O. Manickam and G. M. Homsy, ''Stability of miscible displacements in porous media with nonmonotonic viscosity profiles,'' Phys. Fluids A **5**, 1356 (1993).
[8]O. Manickam and G. M. Homsy, ''Fingering instability in vertical miscible displacement flows in porous media,'' J. Fluid Mech. **288**, 75 (1995).
[9]A. M. Rogerson and E. Meiburg, ''Shear stabilization of miscible displacements in porous media,'' Phys. Fluids A **5**, 1344 (1993).
[10]Y. C. Yortsos, ''Stability of displacement processes in porous media in radial flow geometries,'' Phys. Fluids **30**, 2928 (1987).
[11]C. Pankiewitz and E. Meiburg, ''Miscible porous media displacements in the quarter five-spot configuration. III. Nonmonotonic viscosity profiles,'' J. Fluid Mech. **388**, 171 (1999).
[12]A. Riaz and E. Meiburg, ''Three-dimensional vorticity dynamics of miscible porous media flows,'' J. Turbulence (in press).
[13]M. Ruith and E. Meiburg, ''Miscible rectilinear displacements with gravity override. I. Homogeneous porous medium,'' J. Fluid Mech. **420**, 225 (2000).
[14]H. A. Tchelepi and F. M. Orr, Jr., ''Interaction of viscous fingering, permeability inhomogeneity and gravity segregation in three dimensions,'' SPE Reservoir Eng. November 1994, p. 266.
[15]G. I. Taylor, ''Dispersion of soluble matter in solvent flowing slowly through a tube,'' Proc. R. Soc. London, Ser. A **219**, 186 (1953).
[16]Y. C. Yortsos and M. Zeybek, ''Dispersion driven instability in miscible displacement processes,'' Phys. Fluids **31**, 3511 (1988).
[17]W. B. Zimmerman and G. M. Homsy, ''Nonlinear viscous fingering in miscible displacement with anisotropic dispersion,'' Phys. Fluids A **3**, 1859 (1991).
[18]P. Petitjeans, C.-Y. Chen, E. Meiburg, and T. Maxworthy, ''Miscible quarter five-spot displacements in a Hele-Shaw cell and the role of flow-induced dispersion,'' Phys. Fluids **11**, 1705 (1999).
[19]F. Graf, E. Meiburg, and C. Haertel, ''Density-driven instabilities of miscible fluids in a Hele-Shaw cell: Linear stability analysis of the three-dimensional Stokes equations,'' J. Fluid Mech. **451**, 261 (2002).
[20]D. Wilhelm and E. Meiburg, ''Three-dimensional spectral element simulations of variable density and viscosity, miscible displacements in a capillary tube,'' Comput. Fluids (in press).
[21]C.-Y. Chen and E. Meiburg, ''Miscible porous media displacements in the quarter five-spot configuration. Part 1. The homogeneous case,'' J. Fluid Mech. **371**, 233 (1998).
[22]M. J. Maschhoff and D. C. Sorensen, ''P-ARPACK: An efficient portable large scale eigenvalue package for distributed memory parallel architectures,'' *Applied Parallel Computing in Industrial Problems and Optimization*, Lecture Notes in Computer Science 1184 (Springer, Berlin, 1996).
[23]R. B. Lehoucq, D. C. Sorensen, and C. Yang, ARPACK *USERS GUIDE: Solution of Large Scale Eigenvalue Problems with Implicitly Restarted Arnoldi Methods* (SIAM, Philadelphia, 1998).
[24]S. K. Lele, ''Compact finite differences with spectral-like resolution,'' J. Comput. Phys. **103**, 16 (1992).
[25]F. J. Hickernell and Y. C. Yortsos, ''Linear stability of miscible displacement processes in porous-media in the absence of dispersion,'' Stud. Appl. Math. **74**, 93 (1986).